

Use of RANS for Waterjet Analysis of a High-Speed Sealift Concept Vessel

Keegan Delaney, Martin Donnelly, Michael Ebert & David Fry

Naval Surface Warfare Center – Carderock Division, West Bethesda, MD USA

ABSTRACT

Reynolds Averaged Navier-Stokes (RANS) computational methods are used to analyze waterjet pump performance for two different high speed hull forms. Each hull form is shaped to accommodate unique waterjet pump configurations. Waterjet performance evaluation is based on the International Towing Tank Conference's (ITTC 1996) "momentum and energy flux methods." These flux methods involve analyzing model parameters at six stations throughout the waterjet system, and are used to ultimately predict full scale powering and losses incurred over the waterjet system. Model scale performance parameters at each station can be obtained by traditional experimental practices or computational methods, such as RANS calculations. RANS calculations at certain flow stations within the waterjet system are integrated into experimentally determined powering performance predictions for the entire system. RANS calculations are also used to evaluate assumptions made in experimental practices. RANS full and model scale boundary layers are compared to give further qualitative and quantitative insight into scaling effects. Full scale RANS calculations are also presented and compared to values that are scaled from model scale experimental results. Ultimately, RANS computations predict full scale powering to within two percent of experimentally scaled predictions.

Keywords

Waterjets, Performance, Scaling, RANS, Computations

1 INTRODUCTION

To better understand waterjet performance for high speed surface ships, RANS calculations are performed on the Joint High Speed Sealift (JHSS), which is a monohull concept with four waterjets. Figures 2 and 3 show the JHSS hull form and waterjet inlets. Both bare and powered hull forms are predicted. The waterjet inlets are covered in the bare hull case. The powered predictions are performed with and without the waterjet shafts, both stationary and rotating.

RANS calculations are compared to experimental laser-Doppler velocimetry (LDV) measurements at a model scale. In particular, comparisons are made at Station 1A (located one pump diameter ahead of the inlet tangency),

and Station 3 (located just ahead of the pump). The ITTC standard locations for the flow through the waterjet are indicated in Figure 1.

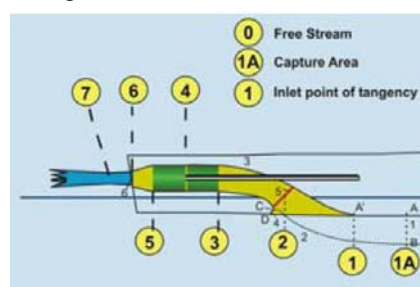


Figure 1. ITTC definitions of control volume analysis stations

Waterjet powering performance is based on the control volume approach proposed by the ITTC, which uses momentum and energy at various stations in the waterjet system to define jet system power and gross jet thrust. The impact of replacing measured parameters with computed values in the derivations of momentum and energy at various stations will be investigated.

This report will include comparisons of RANS calculated waterjet inlet capture areas at Station 1A to previous trapezoidal capture area approximation methods. In prior experimental procedures, inlet capture areas are assumed to be trapezoidal shapes, whose base length and height are calculated based on pump diameter and mass flow rates. However, RANS calculations can be used to track streamlines upstream from the water jet nozzle to Station 1A to computationally determine more realistic capture areas.

Additionally, calculations at Station 3 without the shaft, with a stationary shaft, and with a rotating shaft show the effects of the shaft on the flow field non-uniformity. The Station 3 calculations are also compared with LDV data to examine waterjet performance analysis.

The overall waterjet system control volume performance evaluations are dependent on accurate flowrate determination, quantification of non-uniformity factors, and static pressure measurements. These values can be determined from detailed measurements or RANS calculations. RANS results are integrated into an already

completed waterjet powering performance prediction, and compared to experimental predictions. Additional full-scale Reynolds Number calculations are undertaken to evaluate current inlet wake scaling procedures used to establish full-scale powering predictions from model-scale tow tank experiments.

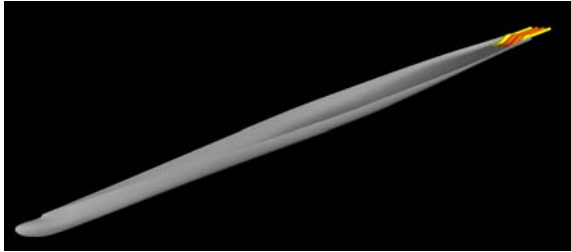


Figure 2. JHSS hull form beneath the water line.

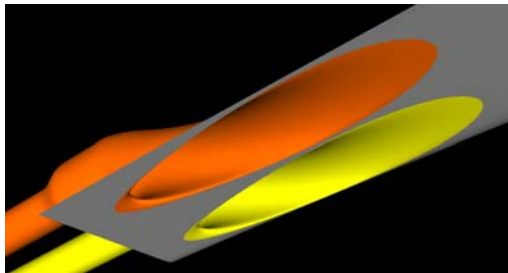


Figure 3. Port side view of the waterjet inlets.

2 FLOW SOLVER AND GRID GENERATION

2.1 Flow Solver

The CFD predicted flow fields used in this work are obtained using the multi-element unstructured, incompressible RANS flow solver TENASI (Sreenivas, Taylor, and Briley 2006) developed at University of Tennessee SimCenter at Chattanooga. The solver is a node-centered, finite volume, implicit scheme that stores the flow variables at the vertices of the grid. The calculations rely on the one-equation Spalart-Allmaras (Spalart and Allmaras 1992) model to account for the effects of turbulence. Subsection 2.3 below describes a turbulence model dependency study that leads to the selection of the Spalart-Allmaras model for this work. The TENASI code is highly parallel and relies on MPI for communicating across multiple processes. Typical calculations used in this work were run over 50-80 processors.

2.2 JHSS Geometry and Grid Generation

This study focuses on the JHSS hull, which is a long, slender hull form. It is approximately 980 ft long with a beam of 105 ft at full scale. Two JHSS variations that both have a gooseneck bow with different transoms are investigated: one which houses 4 axial flow waterjets (referred to as the axial hull) and one which houses 4 mixed flow waterjets (referred to as the mixed hull). Axial flow waterjets can be designed to smaller transom flange diameters than mixed flow waterjets for similar performance specifications. Thus, the axial hull has a narrower and shallower transom with reduced inlet

spacing on the hull. Figure 4 shows the difference between the axial and mixed hull transoms. The prop hull shown in Figure 4 is not included in this work.

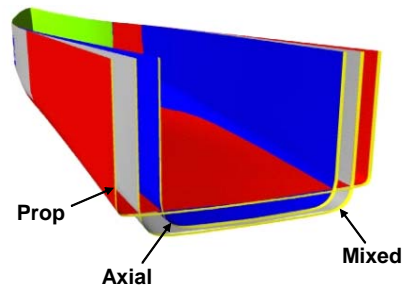


Figure 4. Transom shapes for axial and mixed flow waterjet hulls.

The same surrogate waterjet pumps are used for both the axial and mixed hulls in the experimental study; however, the two hull forms use representative inlet spacing and transom dimensions. Thus, for this study the axial and mixed hull form models have the same geometric waterjet dimensions, but different transoms and inlet spacing on the hulls.

Multi-element unstructured grids are developed using SolidMesh (Gaither 1997), a suite of tools developed at Mississippi State University. SolidMesh provides tools for geometry preparation and surface grid generation. The volume grid is generated by using an advancing normal methodology for the boundary layer prism elements and an Advancing Front/Local Reconnection technique (Marcum and Gaither 1999) to develop high quality isotropic elements. Using these tools, multi-element unstructured grids can be created around complex geometries, like those presented in this work, significantly faster than traditional structured grids. Typical grids used in this study contained 6 to 12 million points for half of the body with port/starboard symmetry assumed.

The hull, waterjet inlets, and shafts are all modeled as viscous surfaces where the first point off the wall is typically a y^+ distance of 1. Prism elements are grown off of all viscous surfaces to capture boundary layer effects. Outside of the boundary layer, the outer region of the flow field is modeled with tetrahedral elements. Figure 5 shows a cross-sectional view of the port side volume grid at Station 3, where prism layers are grown off of the hull, wall of the waterjet inlets, and from the shafts.

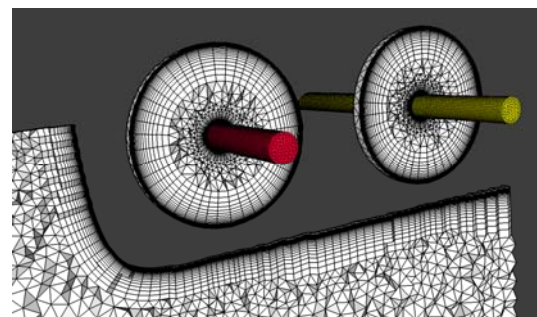


Figure 5. Port cross-sectional view of volume grid at Station 3.

The free surface is treated as a symmetry plane, and the ship is modeled at sinkage and trims prescribed by the propelled experiment. The propelled calculations use an actuator disk model to simulate waterjet propulsion. The disk provides a pressure jump in the axial direction, but does not account for swirl effects. RANS calculations at model scale use experimentally determined volumetric flow rates through the pump as a condition for the thrust provided by the actuator disk model.

The ship is modeled at a full scale forward speed of 36 knots, and the corresponding Reynolds Number based on ship length is $5,330 \times 10^6$. The ship is scaled by a constant Froude Number of 0.347. Model scale conditions correspond to a ship speed of 6.16 knots, and a Reynolds Number based on the ship's length of 26.74×10^6 .

2.3 Bare Hull Grid and Turbulence Model Study

An extensive grid dependency study is done for both the bare and powered hull cases. The grid dependency study consists of varying: point spacing on the hull, boundary layer prism growth, and tetrahedral element size and clustering in the outer flow field. Bare and powered hull grids used in these tests varied from 4 to 14 million points. Figure 6 shows a baseline and refined volume grid cross-section at Station 1A. The refined grid on the right has finer surface spacing on the hull, increased prism layer growth, and finer tetrahedral elements outside the boundary layer. Results presented in this work are from grids that displayed low levels of grid dependency.

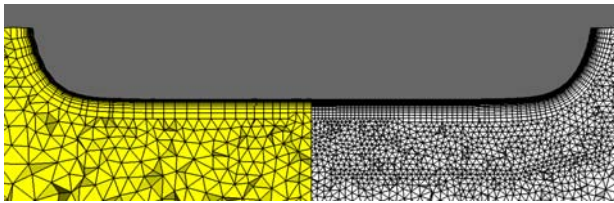


Figure 6. Baseline (L) and refined (R) volume grid cross-sections at Station 1A

A turbulence model dependency study is also done for the axial bare hull case. The Spalart-Allmaras, Menter two-equation $k-\epsilon/k-w$ hybrid (Menter 1994), and Coakley two-equation $q-w$ (Coakley 1983) turbulence models are studied. The Station 1A boundary layers for the different turbulence models are similar. Various Station 1A performance parameters are also calculated for each turbulence model with similar results between the models. Thus, the results presented in this work use the Spalart-Allmaras model.

3 MODEL SCALE STATION 1A RESULTS

Station 1A RANS results are compared with experimental measurements in this section. Station 1A (labeled 1A in Figure 1) is located one inlet diameter upstream from the waterjet inlet tangency point. The capture areas at Station 1A represent the portion of the upstream flow that is ingested into each of the waterjets.

The portion of the boundary layer flow that is ingested into the waterjets significantly affects the waterjet pump efficiency. Typically, the waterjet pump efficiency is higher when lower velocity fluid is ingested.

3.1 Axial Bare Hull Boundary Layer Results

Initially, flow fields are predicted for the axial bare hull case, where the waterjets are not present and the inlets are covered. RANS and experimental bare hull boundary layers can be seen below in Figure 7. All velocity contours presented in this work are non-dimensionalized by ship speed.

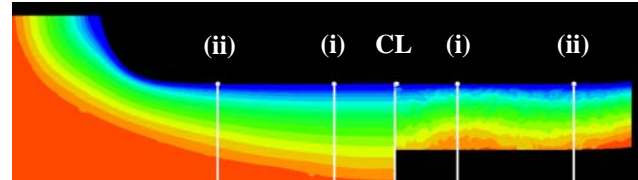


Figure 7. RANS (L) and experimental (R) bare hull Station 1A boundary layers for the axial hull case.

The vertical lines in Figure 7 represent the ship centerline (CL), and where the inboard (i) and outboard (ii) waterjet centerlines would be for the powered hull case. RANS results differ from experiment around the inboard waterjet centerline, and agree more at the centerline and towards the outboard portion of the boundary layer. An important note about Figure 7 is that the inlets are covered on the bare hull, so the experimental flow feature seen around (i) is not related to waterjet suction or inflow.

3.2 Powered Hull Station 1A Capture Areas

Each capture area at Station 1A represents the portion of the flow that is ingested downstream into the respective waterjets. In experiments, the capture areas at Station 1A are assumed to be trapezoids which are sized initially by pump diameter at Station 3 only. The trapezoid is then scaled by a constant factor until the volumetric flow rate through the capture area is equal to the flow rate through the operating pump. However, RANS calculations solve for the entire flow field. Thus, streamlines are tracked upstream from the waterjet pumps to produce stream tubes of the flow that is ingested into the waterjets. Figure 8 shows streamlines tracked upstream from the waterjet inlets intersecting with the incoming boundary layer at Station 1A.

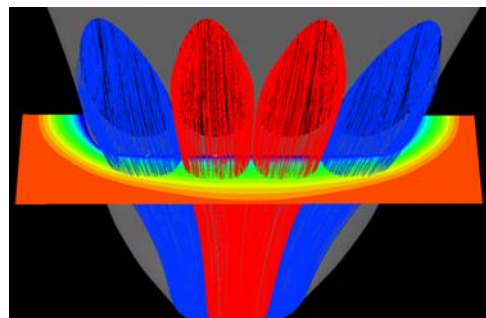


Figure 8. RANS calculated waterjet streamlines (looking aft to fore) intersecting a Station 1A boundary layer.

Then the stream tubes are traced around at the desired location (Station 1A in this case) to determine more realistic capture areas. Figures 9 and 10 show a comparison of experimentally determined and RANS calculated boundary layers and capture areas at Station 1A for the powered axial and mixed hull cases. RANS capture areas are outlined as the rounded grey curves, and the trapezoidal approximations are outlined as the black angular curves. In Figure 9: (i) represents the centerline of the inboard waterjets, (ii) represents the centerline of the outboard waterjets, and (iii) represents an additional outboard location that is referenced later in subsection 3.3.

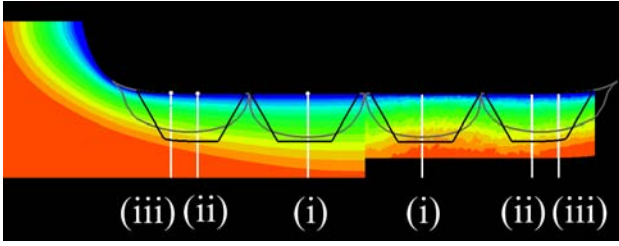


Figure 9. Axial Hull RANS (left) and experimental (right) powered Station 1A boundary layer with capture areas.

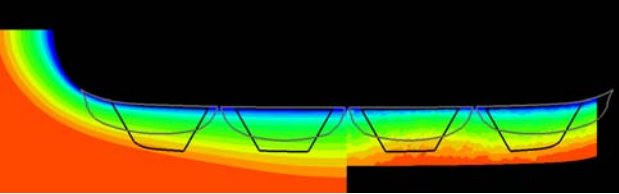


Figure 10. Mixed Hull RANS (left) and experimental (right) powered Station 1A boundary layer with capture areas.

One important note is that LDV measurements of the hull boundary layer were not taken for the mixed hull case. Instead axial hull measurements at Station 1A are fitted to the mixed hull form by matching the profiles at the centerline of each waterjet.

As previously stated, the mixed hull case has a wider and deeper hull with larger inlet spacing on the hull, but the same waterjet inlet geometries are used from the axial case. Figure 11 shows the difference between the axial and mixed hull RANS calculated capture areas.

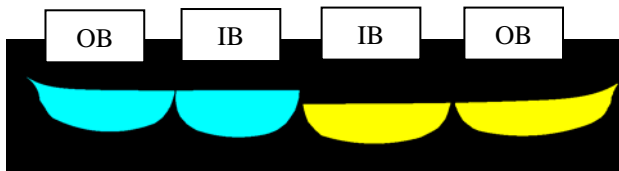


Figure 11. RANS axial (left) and mixed (right) hull Station 1A capture areas.

The experimental procedure for calculating approximate trapezoidal capture areas at Station 1A are based only on

waterjet inlet diameter at Station 3 (D_3). Because the same surrogate pump is used for both axial and mixed hull cases, the inlet diameters at Station 3 are the same for both hulls. However, RANS calculations for the mixed hull show that the capture areas at Station 1A are wider and shallower than the axial hull case that has smaller inlet spacing on the hull. These results show that the previous assumption that capture area dimensions are only dependent on Station 3 pump inlet diameter are incorrect, and that inlet spacing on the hull is an important factor.

The difference in shape between the RANS and trapezoidal capture areas could significantly affect momentum calculations at Station 1A, which would lead to a different gross jet thrust. The momentum at Station 1A is a function of the velocity squared. Thus, if the trapezoidal capture areas are significantly narrower and taller they would consist of higher velocity fluid, which would predict higher momentums at Station 1A and lower overall gross jet thrusts. This conclusion is significant to final performance predictions as the wider, shallower capture area of the mixed flow hull captures more low momentum fluid, improving the efficiency of the pump.

3.3 Station 1A Capture Area Performance Analysis

Relevant Station 1A performance parameters are now compared for the RANS and experimental cases. In the aforementioned control volume approach, the momentum at Station 1A (M_1) is used to calculate jet system thrust force (T) for each waterjet.

$$M_1 = \rho V_{ref} \int V_x \sqrt{\left(\frac{V}{V_{ref}}\right)^2 + C_p} dA_1 \quad (1)$$

$$T = M_7 \cos \alpha - M_1 \quad (2)$$

Where V_{ref} is the ship's speed, C_p is the static pressure coefficient, and A_1 is the Station 1A capture area. M_7 is the momentum at Station 7 located downstream of the nozzle. α is the angle between the nozzle discharge and the shaft axis, which is zero for all calculations in this work.

This subsection will examine the effect of using RANS calculated Station 1A flow fields and capture areas to predict waterjet performance. RANS calculated Station 1A waterjet performance parameters, such as M_1 , are compared directly to experimental Station 1A parameters. The RANS predicted Station 1A parameters are also integrated into overall waterjet system performance equations. Using gross jet thrust as an example, M_7 in Equation 2 would be an experimental value but M_1 would be taken from RANS calculations. This thrust is compared to a thrust calculated with experimental M_1 and M_7 values to analyze the effect of using RANS computations at Station 1A instead of experimental measurements. Tables 1 and 2 show various Station 1A performance parameters for both the axial and mixed hulls compared to measurements.

Table 1. Station 1A RANS (CFD) and experimental (Meas) performance parameters for the axial hull case.

	Inboard			Outboard		
	CFD	Meas	Meas/CFD	CFD	Meas	Meas/CFD
A1 [m ²]	0.00489	0.00442	0.90	0.00474	0.00460	0.97
1-w	0.718	0.785	1.09	0.737	0.760	1.03
β M1	1.015	1.024	1.01	1.017	1.029	1.01
M1 [N]	50.78	54.88	1.08	52.30	54.02	1.03
M7 [N]	97.77	97.77	-	99.53	99.53	-
T [N]	46.99	42.89	0.91	47.23	45.51	0.96

Table 2. Station 1A RANS (CFD) and experimental (Meas) performance parameters for the mixed hull case.

	Inboard			Outboard		
	CFD	Meas	Meas/CFD	CFD	Meas	Meas/CFD
A1 [m ²]	0.00482	0.00446	0.93	0.00466	0.00458	0.98
1-w	0.713	0.770	1.08	0.738	0.748	1.01
β M1	1.015	1.018	1.00	1.018	1.043	1.02
M1 [N]	48.62	52.12	1.07	51.10	52.98	1.04
M7 [N]	96.48	96.48	-	96.67	96.67	-
T [N]	47.86	44.36	0.93	45.57	43.69	0.96

Tables 1 and 2 show the RANS calculated capture areas (A_1) are consistently larger in area and lower in wake fraction ($1-w$) as compared to experimental results. These results are consistent with Figures 9 and 10 which show that the RANS calculated capture areas are relatively wider and more concentrated in the lower velocity portion of the boundary layer.

The value β_{M1} is a momentum non-uniformity factor that is relevant to the experimental procedure for determining momentum at Station 1A.

$$\beta_{M1} = \frac{1}{\bar{V}_1^2} \int V V_x dA_1 \quad (3)$$

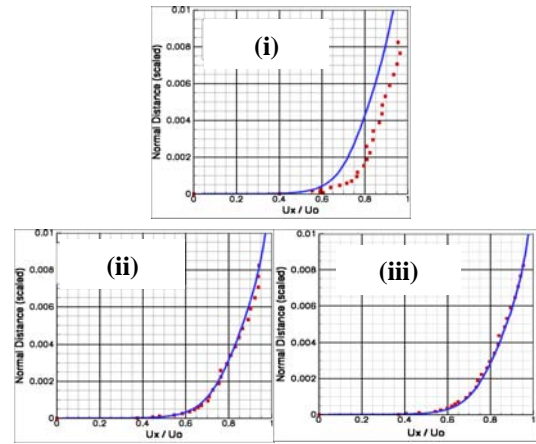
Where \bar{V} is the average velocity in the capture area. Equation 3 shows β_{M1} is unity for a uniform flow field, and deviates from unity as the flow field varies. For RANS computations the momentum at Station 1A is determined by Equation 1 above; however, in common experimental practice the integral terms cannot be determined. Thus Equation 4 represents the experimental procedure for determining momentum at Station 1A.

$$M_1 = \rho Q \bar{V}_1 (\beta_{M1} + \frac{1}{2} C_p) \quad (4)$$

These results show that the momentum non-uniformity factor for these cases is relatively insensitive to changes in the boundary layer when compared to other performance parameters. Even in the inboard areas where the RANS and experimental boundary layers disagree, these non-uniformity factors compare to one percent.

The RANS calculated Station 1A momentum values are lower than experiment, resulting in higher gross jet thrust predictions. The tables also show that there is the best agreement between RANS calculated and experimentally measured results in the outboard capture areas. This is to be expected as there is a distinguished difference in boundary layers around the inboard inlet.

The axial hull case (shown in Figure 9) can be used to further examine the differences that result from using trapezoidal capture area approximations as opposed to RANS calculated areas. In the inboard axial case both the boundary layers and capture areas disagree when comparing RANS and experiment. Thus, for an unknown combination of these two reasons the performance parameters are significantly different. However, around the outboard capture area the boundary layers are relatively similar, but the capture areas have pronounced differences in shape (base width and height). Figures 12-14 quantitatively show RANS and experimental boundary layers normal to the hull at the centerline of the inboard and outboard waterjets (i and ii respectively from Figure 9), as well as an additional outboard location (iii in Figure 9) at Station 1A.



Figures 12-14. Station 1A boundary layer plots for the axial hull at inboard (i) and outboard (ii and iii) locations. The solid lines represent RANS predictions and the square symbols represent measured experimental results.

Figures 12-14 clearly show there is much more agreement between boundary layers around the outboard capture area. These results show that the relatively smaller differences in performance parameters around the outboard capture areas are primarily a result of the different capture area shapes, not the boundary layers. Thus, the difference in quantities in the outboard capture areas are representative of differences that can be expected when using the trapezoidal capture area approximations as opposed to more realistic capture areas.

4 MODEL SCALE STATION 3 AXIAL HULL RESULTS

This section presents results from Station 3, which is located just upstream of the waterjet pump (labeled 3 in Figure 1). Station 3 flow field knowledge is of particular importance, as the delivered pump power (DHP) is directly dependant on Station 3 parameters. Using the control volume approach to analyzing pump performance, Equation 6 shows the energy at Station 3 (E_3 in Equation 5) is used to compute the power delivered by the waterjet pump.

$$E_3 = \frac{1}{2} \rho V_{ref}^2 \int \left(\left(\frac{V}{V_{ref}} \right)^2 + C_{p3} \right) V_x dA_3 \quad (5)$$

$$DHP = \frac{E_5 - E_3}{\eta_{pump}} \quad (6)$$

Where E_5 is the energy at Station 5 (downstream from the pump), and η_{pump} is the waterjet pump efficiency.

RANS calculated results from the powered axial hull case are presented: without the waterjet propeller shaft, with a stationary shaft and with the rotating shaft. Results from these three shaft conditions show the effects of the shaft on Station 3 performance parameters, especially flow non-uniformity factors. Figure 15 shows RANS calculated and experimentally measured Station 3 velocity contour plots for the axial hull.

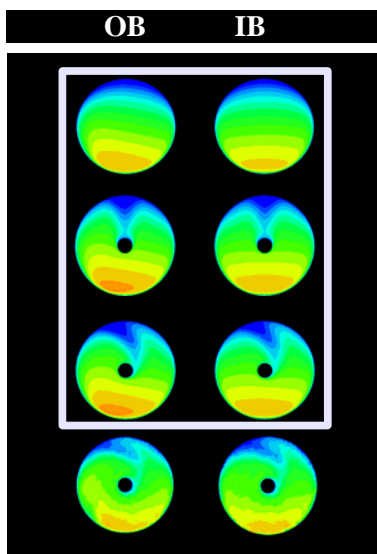


Figure 15. Station 3 velocity contour plots from top to bottom: RANS without a shaft, RANS with stationary shaft, RANS with rotating shaft, and experimental results.

Station 3 RANS results with the rotating shaft compare well with experimental results. Between the three shaft cases (without, stationary, and rotating), the energy non-uniformity factor β_{E3} is of particular interest.

$$\beta_{E3} = \frac{1}{A_3 \bar{V}_3^3} \int V_x^3 dA_3 \quad (7)$$

β_{E3} is a measure of uniformity in the flow field. In CFD calculations the energy at Station 3 is calculated by Equation 5. However, just as in the momentum at Station 1A, in experiments the integrated terms cannot be determined, thus the energy at Station 3 is determined by Equation 8.

$$E_3 = \frac{1}{2} \rho Q \bar{V}_3^2 (\beta_{E3} + C_{p3}) \quad (8)$$

Table 3 shows the effects of the shaft conditions on β_{E3} for the three RANS cases. The first three columns in Table 3 represent RANS calculations without the shaft

(No Shaft), with a stationary shaft (Stat Shaft), and with a rotating shaft (Rot Shaft). The final column in Table 3 represents experimentally measured (Exp Meas) results.

Table 3. Powered axial hull Station 3 RANS (columns 1-3) and experimental (column 4) model parameters for all four waterjets.

	No Shaft	Stat Shaft	Rot Shaft	Exp Meas
Area [m ²]	0.02502	0.02448	0.02448	0.02448
Vbar [m/s]	1.768	1.807	1.804	1.804
betaE	1.223	1.231	1.232	1.172
E3 [W]	114.08	113.08	112.44	112.68
E5 [W]	442.64	442.64	442.64	442.64
n-pump	0.89	0.89	0.89	0.89
DHP [W]	369.17	370.29	371.01	370.74

The results in Table 3 show there is not a significant change in β_{E3} for the three shaft conditions. This is intuitive as the flow field with and without the shaft is essentially the same except for the shaft's wake, and the case with the rotating shaft is the same flow field, only redistributed throughout the area by the rotation. In the end the energy at Station 3 is also similar for all three cases. These results show that adding rotation to the shaft in the CFD model makes the velocity contours match the experimental results well in appearance, but has no quantitative effect on the performance analysis as compared to a stationary shaft.

The energy at Station 5 (E_5) and the pump efficiency (n_{pump}) values in Table 3 are both experimental values. In experimental practice the final model scale delivered pump power (DHP) predicted by the energy flux method is scaled to predict full scale powering. The RANS predicted model DHP for all 3 shaft conditions is similar to the experimental predictions. These results show that there is essentially no difference in predicted model power when substituting RANS calculated values with an experimentally prescribed flow rate for experimentally measured values at Station 3.

5 FULL SCALE RESULTS

This section presents full scale results for the powered axial hull. RANS results are from full scale Reynolds number computations. Because the free surface is modeled as a symmetry plane, model scale RANS predictions iterated on actuator disk thrust until the Station 3 volumetric flow rate matched the measured experimental value. The difference between RANS total ship resistance and the converged actuator disk thrust plus experimental tow force is assumed to be the model scale wave making resistance. The model scale wave making resistance coefficient is assumed to be constant from model to full scale. The constant wave making resistance coefficient is used as a condition to determine full scale actuator disk model thrust. The full scale actuator disk thrust is iterated upon until it is equal to the computed

total ship resistance plus the constant wave drag to simulate self-propulsion.

Experimental model parameters are scaled according to the procedure detailed by Scherer and Wilson (2008) to produce full scale predictions. Inlet wake scaling has not been validated against full-scale measurements. Here, full scale RANS results are compared to model scale results to investigate scaling effects. RANS full scale predictions are also compared to experimentally scaled results.

5.1 RANS Model to Full Scale Comparisons

This subsection presents RANS calculated model and full scale results. Figures 16 and 17 show the difference between RANS model and full scale Station 1A boundary layers. All velocity contours presented in this section are non-dimensionalized by the respective model or full scale ship velocity. All lengths are also scaled by respective model or full scale length between perpendiculars.

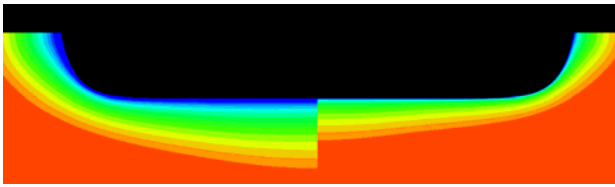


Figure 16. Powered axial hull boundary layer comparisons for model scale (L) and full scale (R) at Station 1A.

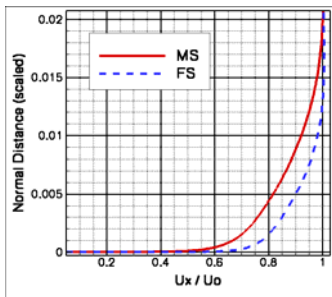


Figure 17. Model scale (solid line) and full scale (dashed line) boundary layer plot normal to hull centerline at Station 1A.

The higher Reynolds number full scale flow produces a significantly thinner non-dimensional velocity boundary layer at Station 1A. The thinner full scale boundary layer will produce greater waterjet thrust efficiency at full scale. Figure 18 shows the differences in model and full scale Station 1A capture areas.

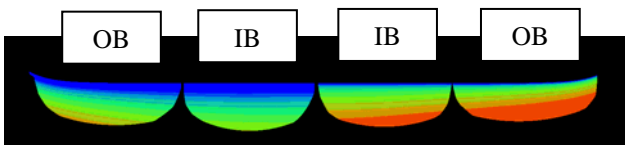


Figure 18. Station 1A powered axial hull capture area comparisons for model scale (L) and full scale (R)

Figure 19 shows the model and full scale Station 3 non-dimensional velocity contour plots. Full scale RANS predictions use a stationary waterjet powering shaft, as Section 4 showed there is no significant advantage to modeling the shaft rotation.

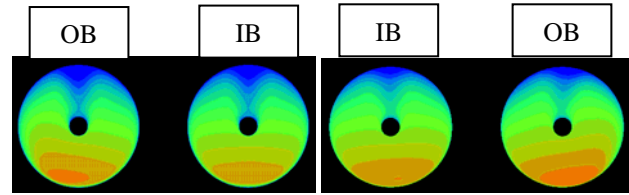


Figure 19. Station 3 powered axial hull capture area comparisons for model scale (L) and full scale (R).

Figure 19 shows that the shaft wake effects are less prominent at full scale. The vertical low velocity band above the shaft is less pronounced for the higher velocity full scale flow.

Inlet efficiency is a measure of losses incurred from flow entering the waterjet inlet; it is calculated by Equation 9.

$$Inlet\ Eff = E_3 / E_1 \quad (9)$$

RANS calculations show that inlet efficiency increases by 6.74 % going from model to full scale. This is most likely due to a reduction in the frictional resistance coefficient, C_f , with increasing Reynolds number. C_f decreased by 49% on the hull from model to full scale. C_f is non-dimensionalized by $\frac{1}{2} \rho U_\infty^2 S$, where S is the wetted surface area. The RANS predicted change in C_f from model to full scale is 2% different than the change predicted by the ITTC 1957 (Hadler 1958) approximation.

Full scale flow field visualization is an additional advantage to integrating RANS calculation into waterjet analysis. RANS results solve for the entire flow field at full scale, while only certain model scale experimental values are scaled. Thus, full scale flow details like boundary layers at Stations 1a and 3 can be visualized to give insight into scaling effects on the flow field.

5.2 RANS and Experimental Full Scale Comparisons

RANS full scale results are compared to experimentally scaled model results in this subsection. It is important to note that RANS full scale computations are run at the full scale Reynolds Number using the procedure described above to determine full scale thrust. While the experimental procedure only scales certain model scale parameters to yield full scale predictions. Table 4 shows comparisons of RANS calculated and experimentally scaled performance parameters.

Table 4. RANS calculated (CFD) and experimentally scaled (Meas) full scale performance parameters for all four waterjets.

	Q @ 1a [cms]	(1-w) @ 1a -	E3 [MW]	E5 [MW]	DHP [MW]
CFD	319.0	0.829	37.35	124.92	98.39
Meas	317.4	0.847	39.10	124.92	96.42
Meas/CFD	0.99	1.02	1.05	1.00	0.98

Where Q is the volumetric flow rate. The RANS predicted wake fraction ($1-w$) is lower than experimentally scaled wake fraction just as in the model scale case. The predicted volumetric flow rates also match very well. In the model scale case the experimental flow rate was a condition for RANS predictions. However, RANS and experiment used different scaling methods to go from model to full scale. These results show that the distinct scaling methods produce relatively small changes in full scale flow rate.

The RANS predicted energy at Station 3 is slightly lower than the experimentally scaled prediction despite having similar volumetric flow rates. These results contrast with the model scale where the E_3 values were indistinguishable. These results would suggest that the experimental scaling procedure is slightly different than the full scale RANS computational methods. Part of this could be due to the RANS predicted β_{E3} decreasing by 2.3% from model to full scale, while experimental procedure assumes it is constant. The ultimate accuracy of either scaling method for this case is unknown.

Despite the difference in predicted energy at Station 3, the final DHP predictions match very well. This agreement can be partially attributed to the fact that the energy at Station 5 is three to four times larger than the energy at Station 3. Thus, the differences at Station 3 get washed out in the final DHP predictions. The main objective for all of these full scale results is to predict full scale powering (DHP). These results show that there is less than one percent difference in DHP when substituting full scale RANS calculations for experimentally scaled results at Station 3.

6 SUMMARY

An extensive study was undertaken to analyze the effect of integrating RANS calculations into experimental waterjet powering predictions. The Station 1A RANS predicted boundary layer differs from experimental measurements around the inboard capture area, but agrees well around the outboard capture area. The difference in RANS and experimentally predicted performance parameters for the outboard capture area is assumed to be the result of different capture area determination techniques. In particular, the two methods results in a four percent difference in predicted gross jet thrust. Experimental practice approximates the capture area at

Station 1A with a trapezoid. The trapezoid is assumed to have dimensions that are a function of waterjet pump diameter and volumetric flow rate at Station 3. RANS calculations suggest that Station 1A capture area sizes are also dependant on other factors, such as inlet spacing on the hull. Also, there is little difference in predicted performance parameters when RANS results are substituted for experimental measurements at Station 3 at both model and full scale. Most importantly, the final RANS and experimental delivered pump power predictions agreed to within one percent at model scale and within two percent at full scale. While the ultimate accuracy of either experimental or RANS method is uncertain, they predicted similar full scale powering using two different techniques.

ACKNOWLEDGEMENTS

This work was funded by the Office of Naval Research, Project Manager Dr. Ki-Han Kim.

REFERENCES

- Coakley, T.J. (1983) 'Turbulence Methods for the Compressible Navier-Stokes Equations.' *AIAA Paper No. 83-1693*.
- Gaither, A.J. (1997). 'A Solid Modeling Topology Data Structure for General Grid Generation.' Master's Thesis, *Mississippi State University*.
- Hadler, J.B. (1958), 'Coefficients for International Towing Tank Conference 1957 Model-Ship Correlation Line.' The David Taylor Model Basin, Report 1185.
- ITTC 1996a (1996). 'Report of the Waterjets Group, Appendix A.' *Proc. of the 21st International Towing Tank Conference*, Bergen and Trondheim Norway.
- Menter, F.R. (1994). 'Two-Equation Eddy Viscosity Turbulence Models for Engineering Applications.' *AIAA Journal* Vol. 32, pp 1598-1605.
- Marcum, D. L., and A. J. Gaither (1999). 'Mixed Element Type Unstructured Grid Generation for Viscous Flow Applications.' *AIAA Paper No. 99-3252*.
- Spalart, P. R. and S. R. Allmaras (1992). 'A one-equation turbulence model for aerodynamic flows.' *AIAA Paper No. 92-0439*.
- Scherer, J.O. and M.B. Wilson (2008). 'Waterjet Inlet Wake Scaling.' NSWCCD Hydromechanics Department Technical Report NSWCCD-50-TR-2008/051
- Sreenivas, K., L.K. Taylor, and W.R. Briley (2006). 'A Global Preconditioner for Viscous Flow Simulations at All Mach Numbers.' *AIAA Paper 2006-3852*.